Acta Crystallographica Section D
Biological Crystallography
ISSN 0907-4449

Metal-free MIRAS phasing: structure of apo-S100A3

Peer R. E. Mittl,[a]* Günter Fritz,[a,b] David F. Sargent,[c] Timothy J. Richmond,[c] Claus W. Heizmann[b] and Markus G. Grütter[a]

[a]Institute of Biochemistry, University of Zurich, Winterthurer Strasse 190, 8057 Zürich, Switzerland, [b]Department of Pediatrics, Division of Clinical Chemistry and Biochemistry, University of Zurich, Steinwiesstrasse 75, 8032 Zürich, Switzerland, and [c]ETH Zurich, Institute of Molecular Biology and Biophysics, ETH-Hönggerberg, 8093 Zurich, Switzerland

Correspondence e-mail: mittl@bioc.unizh.ch

Received 17 January 2002
Accepted 8 May 2002

PDB Reference: apo-S100A3, 1kso, r1ksosf.

S100 proteins are involved in metal-dependent intracellular signalling. Metal-free S100A3, a cysteine-rich Ca^{2+}- and Zn^{2+}-binding protein, has been crystallized by vapour diffusion under the strict exclusion of oxygen and in the absence of divalent metal ions. Metal binding induces large conformational changes, rendering the apo-S100A3 crystals very sensitive to various metal compounds. Therefore, the structure was solved by MIRAS phasing using potassium iodide and xenon derivatives. Iodide replaces a water molecule at the surface of the S100A3 protein, whereas xenon binds in a hydrophobic cavity at the dimer interface. Despite significant non-isomorphism, the combination of both derivatives was sufficient for structure determination. The overall apo-S100A3 structure resembles the structures of metal-free S100B and S100A6 solution structures. In contrast to the NMR structures, the EF-hand loops are well ordered in the apo-S100A3 crystal structure. In the N-terminal pseudo-EF-hand loop a water molecule occupies the position of the Ca^{2+} ion. The C-terminal canonical EF-hand loop shows an extended conformation and a different helix arrangement to other S100/metal complex crystal structures.

1. Introduction

The family of S100 proteins is one of the largest subfamilies of EF-hand calcium-binding proteins (Schäfer & Heizmann, 1996). The individual members of this family show cell- and tissue-specific expression patterns and interact in a Ca^{2+}- and Zn^{2+}-dependent manner with many cellular proteins such as annexin, myosin, intermediate filaments, tau protein and several enzymes including guanylate cyclase and p53. The genes for 13 of the 17 human S100 proteins are localized in a cluster on chromosome 1q21 (Schäfer *et al.*, 1995), a region frequently rearranged in several tumour cell lines. It is supposed that these rearrangements affect the differential expression of S100 proteins as is observed in breast cancer (Albertazzi *et al.*, 1998; Böni *et al.*, 1997; Sastry *et al.*, 1998; Wicki *et al.*, 1997) and several brain-tumour cell lines (Camby *et al.*, 1999, 2000).

S100 proteins have a size of 10–12 kDa and form homodimers or heterodimers (Heizmann & Cox, 1998). The peptide chain folds into a canonical EF-hand at the C-terminus and a non-canonical EF-hand at the N-terminus. Generally, there are four EF-hand metal-binding sites per dimer that are selective for Ca^{2+} ions. Ca^{2+} binding induces a structural change from the closed Ca^{2+}-free to the open Ca^{2+}-loaded conformation. In addition, a number of S100 proteins bind Zn^{2+} ions with a wide range of affinities (K_d = 2–2000 μM) modifying the Ca^{2+} affinities (Föhr *et al.*, 1995). Furthermore, the proteins bind other divalent metal ions, such as Cu^{2+}, Cd^{2+}

Table 1
Statistics of data collection and phasing.

Values in parentheses refer to the outermost shell.

	Native 1	Native 2	Xenon	Potassium iodide
X-ray source	ESRF, beamline ID14-3	Rotating anode	Rotating anode	Rotating anode
Wavelength (Å)	0.934	1.542	1.542	1.542
Resolution (Å)	1.70 (1.76–1.70)	2.00 (2.07–2.00)	2.7 (2.8–2.7)	2.7 (2.8–2.7)
Unit-cell parameters (Å)	$a = b = 58.769$, $c = 45.338$	$a = b = 58.815$, $c = 45.375$	$a = b = 59.731$, $c = 46.749$	$a = b = 59.078$, $c = 46.147$
Unit-cell volume (Å^3)	135609	135932	144445	139484
Mosaicity (°)	0.5	0.6	1.2	0.7
Completeness (%)	98.2 (100)	93.6 (61.3)	86.9 (29.8)	95.8 (69.6)
Observed reflections	34465	41100	16846	24541
Unique reflections	19298	11153	4233	4745
$R_{\rm sym}$ (%)	3.8 (30.0)	6.7 (22.5)	5.8 (17.5)	11.5 (38.3)
$R_{\rm nat}$† (%)	—	—	27.1	19.3
Sites (x, y, z)				
1	—	—	0.3045, 0.0233, −0.0020	0.6168, 0.2669, −0.2360
2	—	—	0.3622, 0.0522, −0.1080	−0.0633, −0.0505, −0.2063
Occupancy				
1	—	—	0.93	0.66
2	—	—	0.96	0.70
B factor (Å^2)				
1	—	—	11.61	30.79
2	—	—	17.29	32.89
Refinement statistics				
Resolution (Å)	20.0–1.7			
R_f	19.4			
$R_{\rm free}$	22.5			
No. of protein atoms	1510			
No. of water molecules	199			

† $R_{\rm nat} = \sum_{hkl} ||F_{\rm deri}(hkl)| - |F_{\rm nat}(hkl)|| / \sum_{hkl} |F_{\rm nat}(hkl)|$.

and Co^{2+}, or lanthanides, such as Eur^{3+}, Tb^{3+} and Yb^{3+}, either to the Zn^{2+}-binding site or into the EF-hand. S100A3 is exceptional among the S100 proteins with regard to its high cysteine content and its metal-binding affinities. Although it shares 35% sequence identity with other members of the S100 family, it binds Ca^{2+} ions with poor affinity (K_d = 4–35 mM) but Zn^{2+} ions with an extraordinarily high affinity (K_d = 2–5 nM). This unique property suggests that S100A3 is regulated by the intracellular Zn^{2+} concentration.

Although a number of high-resolution crystal structures of Ca^{2+}-loaded S100 proteins are available, there is no crystal structure of an S100 protein in the Ca^{2+}-free closed conformation. The major obstacles are most likely to be the high flexibility of the Ca^{2+}-free EF-hand loops and, in the case of S100A3, the reactive cysteine residue content. In order to elucidate the structural determinants for the Ca^{2+} and Zn^{2+} affinities, we have crystallized the S100A3 protein in the absence of oxygen and divalent metal ions and solved the structure by MIRAS phasing using xenon and iodide derivatives.

2. Material and methods

2.1. Protein purification and crystallization

Human S100A3 was expressed recombinantly in *Escherichia coli* and purified under the exclusion of oxygen as described previously (Fritz *et al.*, 1998). The protein has an unusually high content of cysteine residues (ten out of 101 amino acids per monomer), which makes it susceptible to oxidative aggregation and precipitation. Since only 7.5 of the ten cysteine residues were accessible by titration with 5,5′-dithiobis-2-nitrobenzoic acid, the samples were reduced at pH 8.5 prior to crystallization using a tenfold excess of DTT over cysteine content. The sample was incubated for 3 h at 313 K under exclusion of oxygen. In order to avoid reoxidation of S100A3, all subsequent steps were carried out under nitrogen gas in a glove box. The reduced protein was passed through a NAP-5 column (Amersham Pharmacia) equilibrated in 10 mM Tris pH 7.5, eluted in the same buffer and concentrated to 15 mg ml^{-1} by ultrafiltration. To avoid contamination with divalent ions, all buffers were treated with Chelex 100 (Biorad) prior to the adjustment of pH. Chelex 100 resin was added (5 g l^{-1}) and the solution was stirred for 45 min. After adjustment of the pH, the solution was passed through a 0.2 µm filter and stored in plastic bottles. The absence of zinc and calcium ions was verified by atomic absorption spectroscopy.

Crystallization was carried out by the sitting-drop vapour-diffusion method. Drops consisted of 2 µl protein solution mixed with 2 µl of reservoir solution from the commercial Hampton Research crystallization kits Crystal Screen I and II. The crystallization plates were stored in gas-tight Plexiglas boxes and incubated at 293 K. To monitor the absence of oxygen during the crystallization process a small vial containing 0.5 ml of 10% pyrogallol or 0.5 mM reduced methylviologen was included in the Plexiglas box. Crystals were obtained under different conditions using ammonium sulfate as a precipitating agent. Crystals of dimensions up to 0.5 × 0.5 × 0.3 mm grew in the presence of 0.1 M Tris, 1.8 M ammonium sulfate pH 8.3 within 48 h.

2.2. Data collection and phase determination

Prior to data collection, native S100A3 crystals were transferred into a buffer containing the reservoir solution enriched with 30%(v/v) glycerol and flash-frozen in a stream of cold nitrogen gas. Data were collected using Cu $K\alpha$ radiation from an Enraf–Nonius rotating-anode X-ray source, equipped with double-focusing mirrors (ProPhysics, Zürich, Switzerland) and a MAR image-plate detector system. Data were processed and scaled using the *DENZO*/*SCALEPACK* program suite (Otwinowski & Minor, 1997). Crystals belonged

to space group $P3_1$, with unit-cell parameters $a = b = 58.8$, $c = 45.3$ Å and one dimer per asymmetric unit.

Phases were determined using the multiple isomorphous replacement with anomalous dispersion (MIRAS) method. Since the S100A3 protein has a high affinity for various metal ions, heavy-metal salts were unsuitable for forming derivatives because soaking destroyed the crystal lattice. As an alternative we selected potassium iodide (Dauter *et al.*, 2000) and xenon (Schiltz *et al.*, 1995). The iodide derivative was prepared by soaking the crystals in a buffer consisting of 0.5 *M* potassium iodide, 1.5 *M* ammonium sulfate, 30%(*v*/*v*) glycerol, 0.1 *M* Tris pH 8.3 for 30 s and freezing the crystal directly in the cold nitrogen stream. The xenon derivative was prepared using a device similar to that published recently (Sauer *et al.*, 1997). The crystal was transferred from the cryobuffer into humidified xenon gas. After keeping the crystal for 7 min at a xenon pressure of 3 MPa, the crystal was flash-frozen in liquid nitrogen. Data-collection statistics are given in Table 1.

2.3. Structure solution and refinement

Anomalous and isomorphous difference Patterson maps were calculated using the program *CNS* (Brünger *et al.*, 1998). Both anomalous Patterson maps were interpretable, although the map of the xenon derivative was clearer than the map from the iodide derivative (Figs. 1*a* and 1*b*). Each map was interpreted as having two sites that are related by non-crystallographic symmetry. The three data sets collected at the home source were combined and the heavy-atom parameters were refined using the program *SHARP* (Brodersen *et al.*, 2000). The mean figure of merit as a function of resolution is given in Fig. 1(*c*). After solvent flattening, the electron-density map was of reasonable quality and was sufficiently clear to place a previously constructed S100A3 homology model precisely into the density. The model was refined using alternating rounds of manual model building (*O*; Jones *et al.*, 1991) and reciprocal-space refinement (*CNS*). When the synchrotron data set became available, refinement was completed using the program *ARP*/*wARP* (Perrakis *et al.*, 1999). Refinement statistics are given in Table 1. In the final electron-density map all residues except Met1 and the C-terminal residues Ser95–Gln101 were well defined. Figures were prepared using the programs *MOLSCRIPT* (Kraulis, 1991), *BOBSCRIPT* (Esnouf, 1997) and *RENDER* (Merritt & Bacon, 1997).

3. Results and discussion

The S100A3 protein was purified and crystallized under anaerobic conditions and the structure was solved using xenon

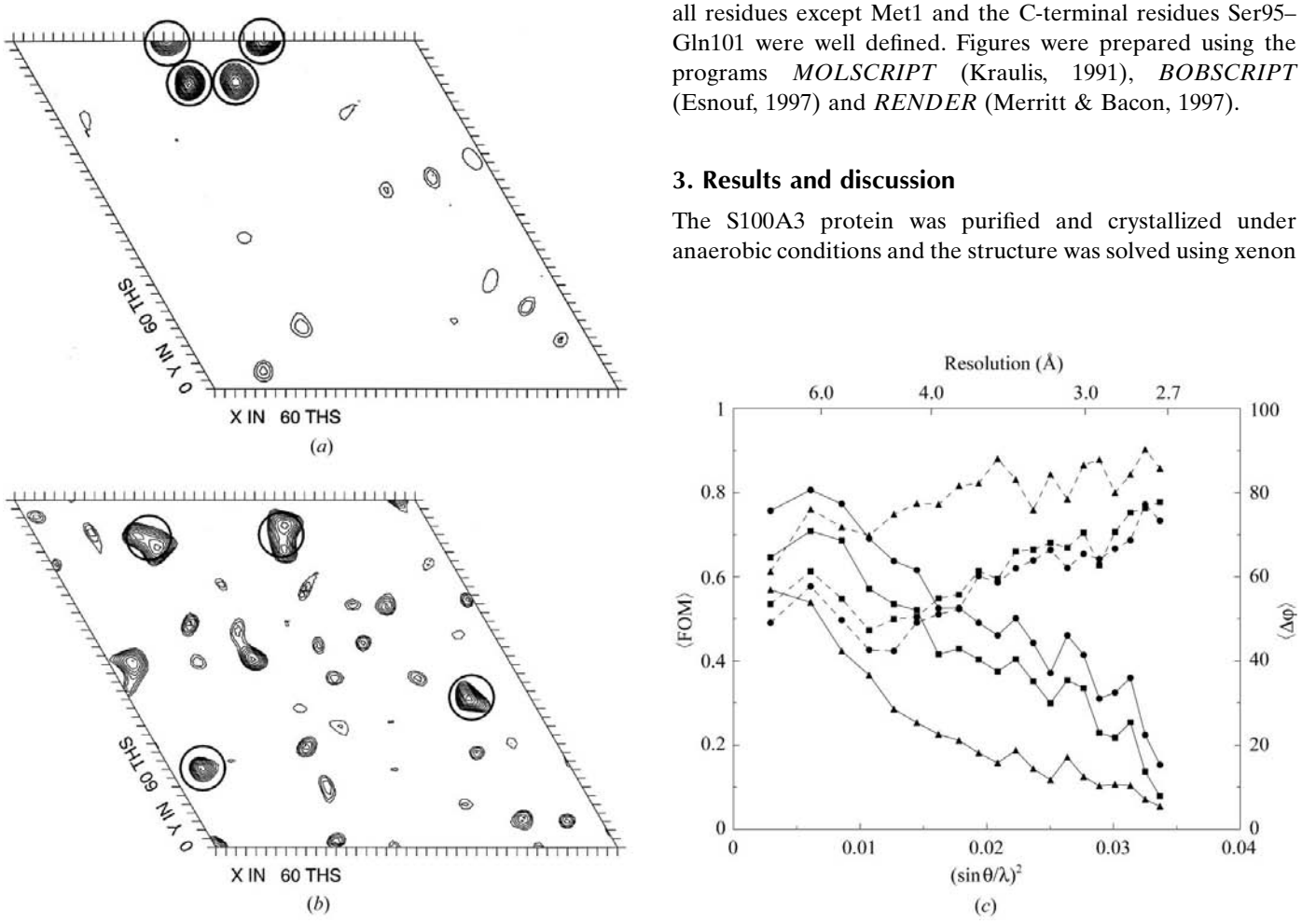

Figure 1
Anomalous Patterson maps of S100A3 xenon (*a*) and potassium iodide derivatives (*b*). Depicted are the asymmetric units (u, v = 0–2/3) of the Harker section (w = 2/3). Maps were calculated with the program *CNS* (Brünger *et al.*, 1998) using data between 30 and 3.0 Å resolution. Peaks that are caused by heavy atoms at the sites given in Table 1 are indicated by circles. (*c*) Mean figures of merit (⟨FOM⟩, solid lines) and mean phase errors between the experimental phases after solvent flattening and the phases calculated from the final structure (⟨Δφ⟩, dashed lines) are plotted as a function of resolution. Triangles, squares and circles refer to the phase sets derived from the single iodide, single xenon and combined iodide/xenon derivatives, respectively.

and iodide derivatives. The application of non-metal compounds was instrumental in structure determination because the crystals were very sensitive to all tested metal compounds. The instability of S100A3 crystals is attributed to their high content of free thiol groups forming high-affinity metal-binding sites and the presence of EF-hand Ca^{2+}-binding sites. There are 20 cysteine residues per S100A3 dimer and all of them are in the reduced state. 16 cysteine side chains are exposed to the solvent (Fig. 2*a*), facilitating direct interactions with the transition metals that are commonly used for the preparation of heavy-atom derivatives. The presence of Ca^{2+}-free EF-hands prevented the application of lanthanides. Since structure solution by molecular replacement was unsuccessful, we selected non-metal compounds for derivatization to circumvent crystal instability. Various non-metal elements suitable for phasing, such as Se, Te, Br, I, Kr and Xe, have been described in the literature. However, the incorporation of Se and Te require modification of the protein prior to crystallization. To obtain suitable anomalous diffraction from Br and Kr derivatives synchrotron radiation is required. The real and imaginary parts of the atomic scattering factors for I and Xe at the Cu $K\alpha$ wavelength are $\Delta f' = -0.58/\Delta f'' = 6.84$ and $\Delta f' = -0.78/\Delta f'' = 7.35$, respectively, giving rise to reasonable anomalous signals for X-ray diffraction data collected at the home source.

Both derivatives indeed show significant isomorphous and anomalous signals and the anomalous Patterson map of the xenon derivative is particularly easily interpretable, but the derivatives also show a considerable amount of non-isomorphism as indicated by the 6.5 and 2.9% increase of the unit-cell volume upon binding of xenon and iodide, respectively. In Fig. 1(*c*) the mean phase error and the mean figure of merit is plotted as a function of resolution. Taken on its own, the iodide derivative is very poor, yielding an almost non-interpretable map with a mean phase error of 81°. However, in combination with the xenon derivative the mean figure of merit is significantly improved, yielding a poor but interpretable map with a mean phase error of 58°.

The anomalous difference Fourier maps for the xenon and iodide derivatives are shown in Fig. 2(*a*). Both Xe atoms bind at the dimer interface close to the twofold NCS axis in a chiefly hydrophobic environment. The xenon-binding sites are only 6.02 Å apart and are completely shielded from the solvent. The binding sites are formed by the side chains of residues Val9, Ile12, Phe72, Val76, Leu79 and Ala80 (Fig. 2*b*). In the final S100A3 crystal structure these residues enclose a cavity with a volume of 39 Å^3. The volume of this cavity would be sufficient to host a Xe atom, but the distance between the Xe atom and Ile*B*12 CD1 is only 2.32 Å, which would be too short for a van der Waals contact (Fig. 2*b*). Since Ile12 is very close to the twofold axis that relates chains *A* and *B*, the side chain of Ile*A*12 points towards Ile*B*12. To avoid a clash between side chains, the χ_1 angles of Ile12 in chains *A* and *B* are −73 and 81°, respectively. Therefore, Ile*B*12 CD1 points into the cavity that is occupied by the xenon in the heavy-atom derivative, whereas Ile*A*12 CD1 points towards subunit *B* (Fig. 2*b*). However, this asymmetry is not seen in the xenon derivative, because two Xe atoms bind to the S100A3 dimer simultaneously, as judged by the occupancies and *B* factors of the refined Xe atoms (Table 1). Occupation of both sites is only possible if Ile12 changes its conformation introducing considerable non-isomorphism and ultimately poor electron density. A different conformation of Ile*B*12 in the S100A3/Xe complex is also suggested by strong negative

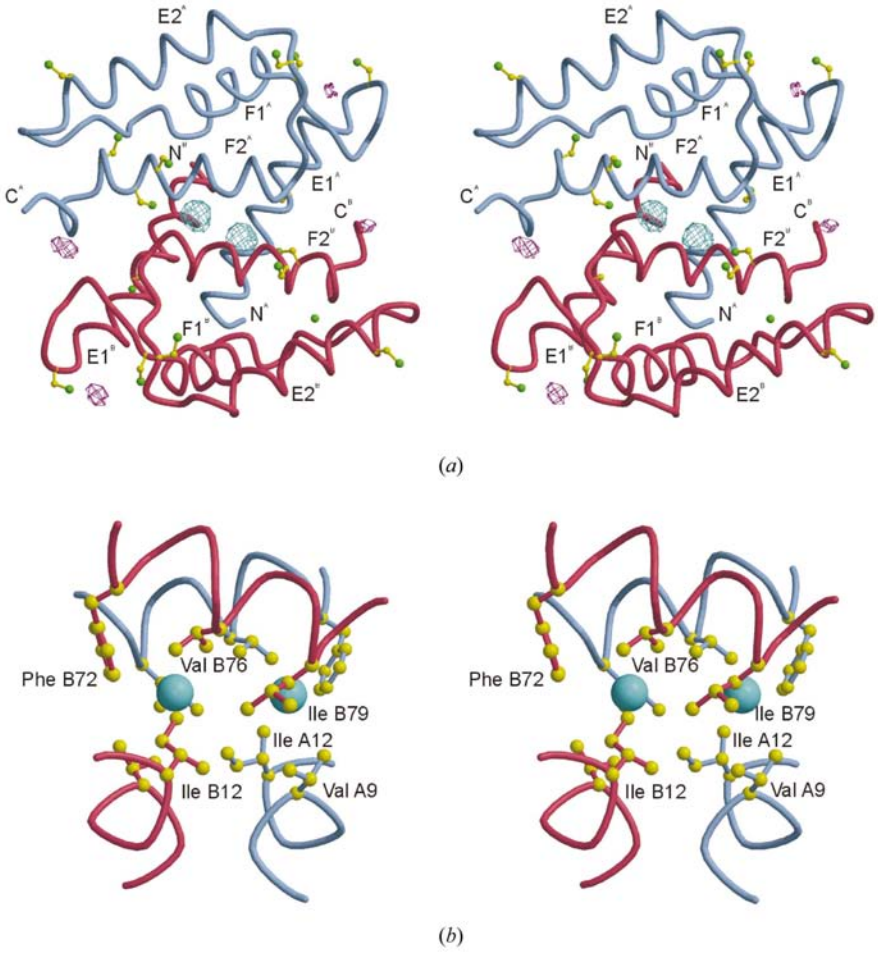

Figure 2
(*a*) Stereo diagram of the S100A3 dimer viewed along the twofold axis. Depicted are chains *A* (blue) and *B* (red), cysteine residues and anomalous difference maps of the xenon (cyan) and iodide (magenta) derivatives. Maps were contoured at 5σ. (*b*) Binding site of the Xe atoms at the dimer interface.

electron density in the $F_o^{Xe} - F_c$ map at the position of atom Ile*B*12 CD1. In contrast to the Xe atoms, the iodide binds at the molecular surface close to a crystal contact. The binding sites are related by the NCS and close to the C-termini of helices E1^A and F2^B (the superscripts *A* and *B* refer to the NCS-related molecules *A* and *B*). There are no obvious reasons why iodide binds selectively to these sites, as the binding sites are very shallow and there are no hydrogen bonds between the ion and the protein. The electrostatic potential of this site is neutral, because the contributions of Arg*A*22 and His*B*87 and the helix dipole moments of helices E1^A and F2^B compensate each other.

The crystal structure of apo-S100A3 is most similar to the solution structures of Ca^{2+}-free S100B (r.m.s.d. 3.4 Å; Drohat *et al.*, 1999) and S100A6 (r.m.s.d. 3.2 Å; Potts *et al.*, 1995), but is different from all other S100 crystal structures. The structural differences are attributed to the binding of metal ions. In apo-S100A3 the angles between helices E1 and F1 that create the N-terminal pseudo-EF-hands are 30°, whereas helices E2 and F2 that create the C-terminal canonical EF-hands are aligned approximately collinearly (Fig. 3*a*). These packing angles are similar in the NMR structures of metal-free S100B and S100A6, but are different in the crystal structures of S100 proteins complexed with calcium (Fig. 3*b*). Metal binding induces a conformational change in the canonical EF-hand that is responsible for signal propagation. In S100 metal complexes such as the S100B/Ca^{2+} complex (Kilby *et al.*, 1996), helices from the pseudo-EF-hands and canonical EF-hands adopt packing angles of 30 and 95°, respectively. In contrast to the metal-free solution structures that possess a high degree of flexibility in the EF-hand loops, these loops are very stable and well ordered in the apo-S100A3 crystal structure as indicated by the low temperature factors.

The pseudo-EF-hand loops in the apo-S100A3 structure (residues 22–33) and the S100B/Ca^{2+} complex (residues 20–31) adopt similar conformations (Fig. 4*a*). In the apo-S100A3 structure water molecules (Wat1, Wat6) occupy the position of the calcium ion. There is no indication that these water molecules might actually be a metal ion since their temperature factors are similar to the temperature factors of the surrounding peptide atoms. The water molecules form direct hydrogen bonds with Ala20 O (3.10 and 3.13 Å), Cys23 O (2.87 and 2.84 Å), Asp25 O (2.77 and 2.96 Å), Cys28 O (2.86 and 2.76 Å), and water-mediated hydrogen bonds with the side chain of Glu33. In the apo-S100A3 crystal structure the Ca^{2+}-binding site is preformed and slightly more open than in the S100B/Ca^{2+} complex, perhaps owing to the absence of direct hydrogen bonds between Wat1 and Glu33.

In contrast to the pseudo-EF-hand that is already in the proper conformation for metal binding, the conformation of the canonical EF-hand is substantially different in the apo-S100A3 and S100B/Ca^{2+} complex (Kilby *et al.*, 1996) structures (Fig. 4*b*). In the apo-S100A3 structure residues 63–74 form an extended loop. A superposition of the apo-S100A3 and S100B/Ca^{2+} complex structures based on the entire subunits reveals that helix F1 of the canonical EF-hands superimpose very well. However, Cys68 is in a β-sheet conformation in the apo-S100A3 structure and the corresponding residue in the S100B/Ca^{2+} complex (Gly66) is in the left-handed helix conformation. In the S100B/Ca^{2+} complex the Ca^{2+} ion interacts with Asp61 OD1, Asp63 OD1, Asp65 OD1, Glu67 O and the side chain of Glu72 from the canonical EF-hand. The positive charge of the Ca^{2+} ion counterbalances

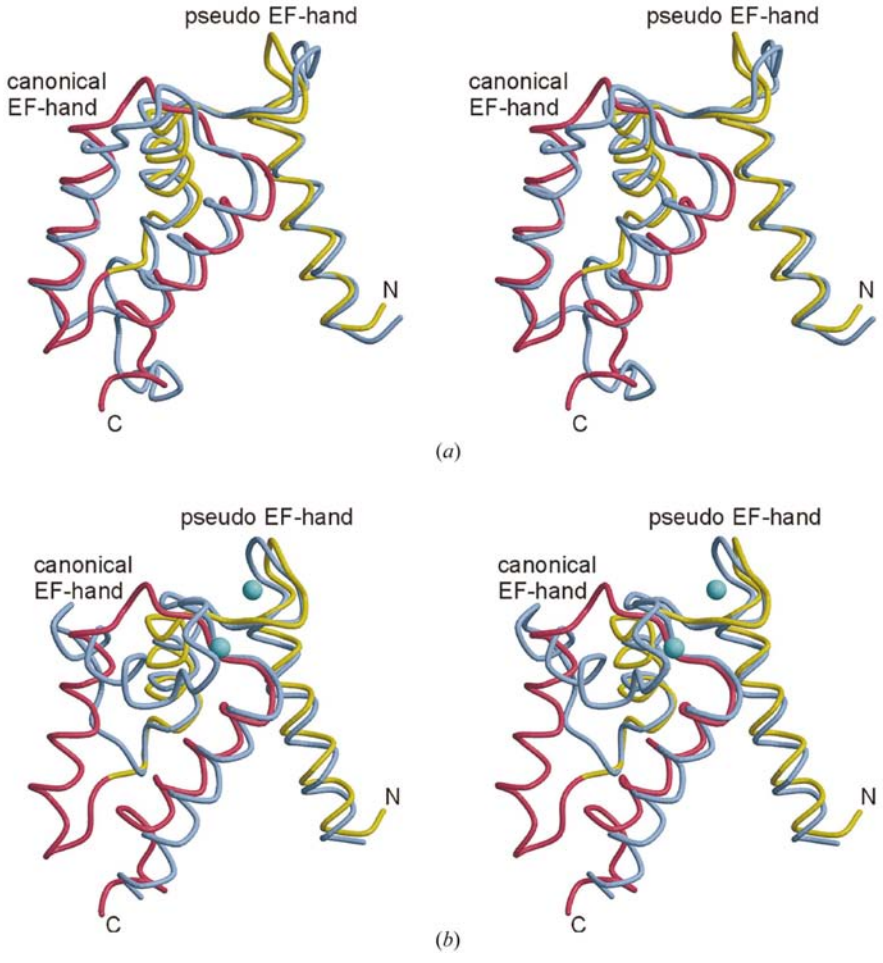

Figure 3
(*a*) Stereo diagram of the superposition of the apo-S100A3 monomer on the metal-free S100B NMR structure (light blue; PDB code 1b4c; Drohat *et al.*, 1999). The N-terminal pseudo-EF-hand and the C-terminal canonical EF-hand are shown in yellow and red, respectively. (*b*) Superposition of the apo-S100A3 structure onto the S100B/Ca^{2+} complex structure (light blue; PDB code 1mho; Kilby *et al.*, 1996).

the electrostatic repulsion of residues Asp61, Asp63, Asp65, Glu67, Asp69 and Glu72, allowing the side chains to come close together in space. Since this counter-ion is missing in the apo-S100A3 structure, the electrostatic repulsion between the side chains of Asp63, Asp67, Glu69, Asp71 and Glu74 forces an extended loop conformation and ultimately the different relative orientations of helices E2 and F2 from the canonical EF-hand. The different conformational changes of pseudo- and canonical EF-hands are explained by the different modes of protein–metal interactions. In the pseudo-EF-hand the Ca^{2+} ion is recognized mainly by uncharged main-chain atoms; therefore, the repulsive forces are less strong and the pseudo-EF-hand can stay in a closed conformation even in the apo-protein. The negatively charged side chains in the canonical EF-hand exert a stronger electrostatic repulsion in the apo-protein, causing a large conformational change of the canonical EF-hand upon Ca^{2+} binding.

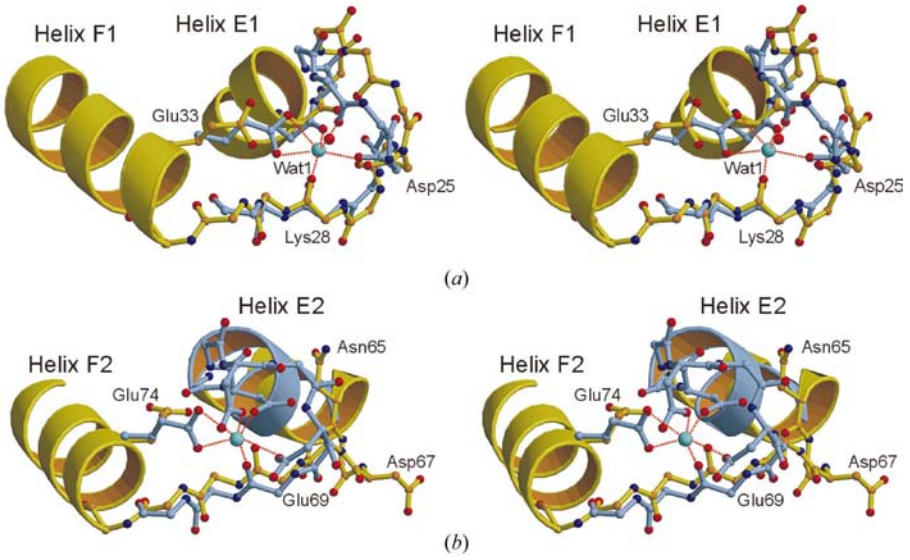

Figure 4
Superposition of the pseudo-EF-hands (*a*) and canonical EF-hands (*b*) of apo-S100A3 (yellow) and S100B/Ca^{2+} complex (light blue) (Kilby *et al.*, 1996). Ca^{2+} ions and water molecules are shown as light blue and red spheres, respectively. Polar interactions between the Ca^{2+} ions and the S100B protein are depicted as red dashed lines. Only selected side chains are shown. Residue numbering refers to the apo-S100A3 structure.

The apo-S100A3 structure illustrates that the combination of iodide and xenon derivatives is of great advantage, particularly for proteins that contain metal-binding sites. Filling these sites with heavy metals for phase determination often leads to crystal damage owing to the strong effects of the metals on the electrostatic potentials of the proteins or owing to conformational changes. In contrast to many metal compounds that occupy similar sites in protein structures, the determinants for xenon- and iodide-binding sites are completely different. Xenon prefers narrow hydrophobic cavities that are inaccessible to the solvent, whereas iodide replaces water molecules on the surface of the protein. The combination of non-metal compounds, particularly xenon and iodide, is a powerful tool for MIRAS phasing, particularly for the apo-forms of metal-binding proteins.

Note added in proof. After this manuscript was accepted for publication, Otterbein *et al.* (2002) reported the crystal structures of S100A6 in the Ca^{2+}-free and Ca^{2+}-bound states. Their results agree with our findings reported above.

The technical support of Drs Julien Lescar and Ed Mitchell during data collection on station ID14-3 (ESRF, Grenoble. France) and Dr Clemens Vonrhein (Global Phasing Ltd, Cambridge) for fruitful discussions on heavy-atom refinement is acknowledged. This work was supported by the Swiss National Science Foundation and the Baugarten Stiftung (Zürich, Switzerland). GF acknowledges a postdoctoral fellowship from the Deutsche Forschungsgemeinschaft and from the Wilhelm-Sander Stiftung.

References

Albertazzi, E., Cajone, F. & Sherbet, G. V. (1998). *DNA Cell Biol.* **17**, 1003–1008.
Böni, R., Burg, G., Doguoglu, A., Ilg, E. C., Schäfer, B. W., Muller, B. & Heizmann, C. W. (1997). *Br. J. Dermatol.* **137**, 39–43.
Brodersen, D. E., de La Fortelle, E., Vonrhein, C., Bricogne, G., Nyborg, J. & Kjeldgaard, M. (2000). *Acta Cryst.* D**56**, 431–441.
Brünger, A. T., Adams, P. D., Clore, G. M., DeLano, W. L., Gros, P., Grosse-Kunstleve, R. W., Jiang, J. S., Kuszewski, J., Nilges, M., Pannu, N. S., Read, R. J., Rice, L. M., Simonson, T. & Warren, G. L. (1998). *Acta Cryst.* D**54**, 905–921.
Camby, I., Lefranc, F., Titeca, G., Neuci, S., Fastrez, M., Dedecken, L., Schäfer, B. W., Brotchi, J., Heizmann, C. W., Pochet, R., Salmon, I., Kiss, R. & Decaestecker, C. (2000). *Neuropathol. Appl. Neurobiol.* **26**, 76–90.
Camby, I., Nagy, N., Lopes, M. B., Schäfer, B. W., Maurage, C. A., Ruchoux, M. M., Murmann, P., Pochet, R., Heizmann, C. W., Brotchi, J., Salmon, I., Kiss, R. & Decaestecker, C. (1999). *Brain Pathol.* **9**, 1–19.
Dauter, Z., Dauter, M. & Rajashankar, K. R. (2000). *Acta Cryst.* D**56**, 232–237.
Drohat, A. C., Tjandra, N., Baldisseri, D. M. & Weber, D. J. (1999). *Protein Sci.* **8**, 800–809.
Esnouf, R. M. (1997). *J. Mol. Graph.* **15**, 132–134.
Föhr, U. G., Heizmann, C. W., Engelkamp, D., Schäfer, B. W. & Cox, J. A. (1995). *J. Biol. Chem.* **270**, 21056–21061.
Fritz, G., Heizmann, C. W. & Kroneck, P. M. (1998). *Biochim. Biophys. Acta*, **1448**, 264–276.
Heizmann, C. W. & Cox, J. A. (1998). *Biometals*, **11**, 383–397.
Jones, T. A., Zou, J. Y., Cowan, S. W. & Kjeldgaard, M. (1991). *Acta Cryst.* A**47**, 110–119.
Kilby, P. M., Van Eldik, L. J. & Roberts, G. C. (1996). *Structure*, **4**, 1041–1052.
Kraulis, P. J. (1991). *J. Appl. Cryst.* **24**, 946–950.
Merritt, E. A. & Bacon, D. J. (1997). *Methods Enzymol.* **277**, 505–524.
Otterbein, L. R., Kordowska, J., Witte-Hoffmann, C., Wang, C. L. & Dominguez, R. (2002). *Structure*, **10**, 557–567.

Otwinowski, Z. & Minor, W. (1997). *Methods Enzymol.* **276**, 307–326.
Perrakis, A., Morris, R. & Lamzin, V. S. (1999). *Nature Struct. Biol.* **6**, 458–463.
Potts, B. C., Smith, J., Akke, M., Macke, T. J., Okazaki, K., Hidaka, H., Case, D. A. & Chazin, W. J. (1995). *Nature Struct. Biol.* **2**, 790–796.
Sastry, M., Ketchem, R. R., Crescenzi, O., Weber, C., Lubienski, M. J., Hidaka, H. & Chazin, W. J. (1998). *Structure*, **6**, 223–231.
Sauer, O., Schmidt, A. & Kratky, C. (1997). *J. Appl. Cryst.* **30**, 476–486.
Schäfer, B. W. & Heizmann, C. W. (1996). *Trends Biochem. Sci.* **21**, 134–140.
Schäfer, B. W., Wicki, R., Engelkamp, D., Mattei, M. G. & Heizmann, C. W. (1995). *Genomics*, **25**, 638–643.
Schiltz, M., Fourme, R., Broutin, I. & Prangé, T. (1995). *Structure*, **3**, 309–316.
Wicki, R., Franz, C., Scholl, F. A., Heizmann, C. W. & Schäfer, B. W. (1997). *Cell Calcium*, **22**, 243–254.